LAWRENCE
LIVERMORE
NATIONAL
LABORATORY

LLNL-JRNL-574772

Triple-wavelength, narrowband Mg/SiC multilayers with corrosion resistance and high peak reflectance in the 25-80 nm wavelength region

M. Fernandez Perea, E. T. Al

August 17, 2012

Optics Express

Disclaimer

Triple-wavelength, narrowband Mg/SiC multilayers with corrosion resistance and high peak reflectance in the 25-80 nm wavelength region

Mónica Fernández-Perea,[1] Regina Soufli,[1,*] Jeff C. Robinson,[1] Luis Rodríguez-De Marcos,[2] Jose A. Méndez,[2] Juan I. Larruquert,[2] and Eric M. Gullikson[3]

[1]Lawrence Livermore National Laboratory, 7000 East Avenue, Livermore, CA 94550, USA
[2]Instituto de Óptica, Consejo Superior de Investigaciones Científicas, C/ Serrano 144, 28006 Madrid, Spain
[3]Lawrence Berkeley National Laboratory, 1 Cyclotron Road, Berkeley, CA 94720, USA
[*]regina.soufli@llnl.gov

Abstract: We have developed new, corrosion-resistant Mg/SiC multilayer coatings which can be used to efficiently and simultaneously reflect extreme ultraviolet (EUV) radiation in single or multiple narrow bands centered at wavelengths in the spectral region from 25 to 80 nm. Corrosion mitigation is achieved through the use of partially amorphous Al-Mg thin layers. Three different multilayer design concepts were developed and deposited by magnetron sputtering and the reflectance was measured at near-normal incidence in a broad spectral range. Unprotected Mg/SiC multilayers were also deposited and measured for comparison. They were shown to efficiently reflect radiation at a wavelength of 76.9 nm with a peak reflectance of 40.6% at near-normal incidence, the highest experimental reflectance reported at this wavelength for a narrowband coating. The demonstration of multilayer coatings with corrosion resistance and multiple-wavelength EUV performance is of great interest in the development of mirrors for space-borne solar physics telescopes and other applications requiring long-lasting coatings with narrowband response in multiple emission lines across the EUV range.

OCIS codes: (310.4165) Multilayer design; (260.7200) Ultraviolet, extreme; (230.4040) Mirrors; (310.1860) Deposition and fabrication; (350.6090) Space optics

References and Links

1. A. B. C. Walker, Jr., J. F. Lindblom, T. W. Barbee, Jr., and R. B. Hoover, "Soft X-ray Images of the Solar Corona with a Normal-Incidence Cassegrain Multilayer Telescope", Science **241**, 1781-1787 (1988).
2. B. De Pontieu, S. W. McIntosh, M. Carlsson, V. H. Hansteen, T. D. Tarbell, P. Boerner, J. Martinez-Sykora, C. J. Schrijver, and A. M. Title, "The Origins of Hot Plasma in the Solar Corona", Science **331**, 55-58 (2011).
3. S. P. Hau-Riege, H. N. Chapman, J. Krzywinski, R. Sobierajski, S. Bajt, R. A. London, M. Bergh, C. Caleman, R. Nietubyc, L. Juha, J. Kuba, E. Spiller, S. Baker, R. Bionta, K. Sokolowski Tinten, N. Stojanovic, B. Kjornrattanawanich, E. M. Gullikson, E. Plönjes, S. Toleikis, and T. Tschentscher, "Subnanometer-Scale Measurements of the Interaction of Ultrafast Soft X-Ray Free-Electron-Laser Pulses with Matter," Phys. Rev. Lett. **98**, 145502 (2007).
4. S. Heinbuch, M. Grisham, D. Martz, and J. J. Rocca, "Demonstration of a desk-top size high repetition rate soft x-ray laser," Opt. Express **13**, 4050-4055 (2005).
5. J. Filevich, K. Kanizay, M.C. Marconi, J.L.A. Chilla, and J.J. Rocca, "Dense plasma diagnostics with an amplitude-division soft-x-ray laser interferometer based on diffraction gratings," Opt. Lett. **25**, 356-358 (2000).
6. I. A. Artioukov, B.R. Benware, J.J. Rocca, M. Forsythe, Y.A. Uspenskii, and A.V. Vinogradov, "Determination of XUV optical constants by reflectometry using a high-repetition rate 46.9-nm laser," IEEE J. Sel. Top. Quantum Electron. **5**, 1495-1501 (1999).

7. M. Seminario, J.J. Rocca, R. Depine, B. Bach, and B. Bach, "Characterization of Diffraction Gratings by use of a Tabletop Soft-X-Ray Laser," Appl. Opt. **40**, 5539-5544 (2001).
8. J. Shin, F. Dong, M. E. Grisham, J. J. Rocca, and E. R. Bernstein, "Extreme ultraviolet photoionization of aldoses and ketoses," Chem. Phys. Lett. **506**, 161-166 (2011).
9. P. Wachulak, M. Grisham, S. Heinbuch, D. Martz, W. Rockward, D. Hill, J. J. Rocca, C. S. Menoni, E. Anderson, and M. Marconi, "Interferometric lithography with an amplitude division interferometer and a desktop extreme ultraviolet laser," J. Opt. Soc. Am. B **25**, B104-B107 (2008).
10. C. Brewer, F. Brizuela, P. Wachulak, D. Martz, W. Chao, E. Anderson, D. Attwood, A. Vinogradov, I. Artyukov, A. Ponomareko, V. Kondratenko, M. Marconi, J. Rocca, and C. Menoni, "Single-shot extreme ultraviolet laser imaging of nanostructures with wavelength resolution," Opt. Lett. **33**, 518-520 (2008).
11. C. Hecquet, F. Delmotte, M.-F. Ravet-Krill, S. de Rossi, A. Jérome, F. Bridou, F. Varnière, E. Meltchakov, F. Auchère, A. Giglia, N. Mahne, and S. Nannarone, "Design and performance of two-channel EUV multilayer mirrors with enhanced spectral selectivity," Appl. Phys. A **95**, 401-408 (2009).
12. T. Ejima, Y. Kondo, M. Watanabe, "Two-Color Reflection Multilayers for He-I and He-II Resonance Lines for Microscopic Ultraviolet Photoelectron Spectroscopy Using Schwarzschild Objective," Jpn. J. Appl. Phys. **40**, 376-379 (2001).
13. P. Boerner, C. Edwards, J. Lemen, A. Rausch, C. Schrijver, R. Shine, L. Shing, R. Stern, T. Tarbell, A. Title, C. J. Wolfson, R. Soufli, E. Spiller, E. Gullikson, D. McKenzie, D. Windt, L. Golub, W. Podgorski, P. Testa, and M. Weber, "Initial calibration of the Atmospheric Imaging Assembly (AIA) on the Solar Dynamics Observatory (SDO)," Solar Physics **275**, 41-66 (2012).
14. R. Soufli, D. L. Windt, J. C. Robinson, S. L. Baker, E. A. Spiller, F. J. Dollar, A. L. Aquila, E. M. Gullikson, B. Kjornrattanawanich, J. F. Seely, and L. Golub, "Development and testing of EUV multilayer coatings for the atmospheric imaging assembly instrument aboard the Solar Dynamics Observatory ," SPIE Proc. **5901**, 59010M (2005).
15. R. Soufli , E. Spiller, D. L. Windt, J. C. Robinson, E. M. Gullikson, L. Rodriguez-de Marcos, M. Fernández-Perea, S. L. Baker, A. L. Aquila, F. J. Dollar, J. A. Méndez, J. I. Larruquert, L. Golub, and P. Boerner, "In-band and out-of-band reflectance calibrations of the EUV multilayer mirrors of the Atmospheric Imaging Assembly instrument aboard the Solar Dynamics Observatory", SPIE Proc. **8443** (2012).
16. D. Martínez-Galarce, R. Soufli, D. L. Windt, M. Bruner, E. Gullikson, S. Khatri, E. Spiller, J. Robinson, S. Baker, and E. Prast, "Microroughness measurements and EUV calibration of the Solar Ultraviolet Imager multilayer-coated mirrors", SPIE Proc. **8501** (2012).
17. H. Takenaka, S. Ichimaru, T. Ohchi, and E. M. Gullikson, "Soft-X-ray reflectivity and heat resistance of SiC/Mg multilayer," J. Electron Spectrosc. Relat. Phenom. **144-147**, 1047-1049 (2005).
18. A. Aquila, F. Salmassi, Y. Liu, and E. M. Gullikson, "Tri-material multilayer coatings with high reflectivity and wide bandwidth for 25 to 50 nm extreme ultraviolet light," Opt. Express **17**, 22102-22107 (2009).
19. D. L. Windt, S. Donguy, J. Seely, and B. Kjornrattanawanich, "Experimental Comparison of Extreme-Ultraviolet Multilayers for Solar Physics," Appl. Opt. **43**, 1835-1848 (2004).
20. S. A. Yulin, F. Schaefers, T. Feigl, and N. Kaiser, "Enhanced reflectivity and stability of Sc/Si multilayers," SPIE Proc. **5193**, 155-163 (2004).
21. D. L. Windt and J. A. Bellotti, "Performance, structure, and stability of SiC/Al multilayer films for extreme ultraviolet applications," Appl. Opt. **48**, 4932-4941 (2009).
22. J. Zhu, S. Zhou, H. Li, Q. Huang, Z. Wang, K. Le Guen, M. Hu, J. André, P. Jonnard, "Comparison of Mg-based multilayers for solar He II radiation at 30.4 nm wavelength," Appl. Opt. **49**, 3922-3925 (2010).
23. M. Vidal-Dasilva, M. Fernández-Perea, J. A. Méndez, J. A. Aznárez, J. I. Larruquert, "Narrowband multilayer coatings for the extreme ultraviolet range of 50-92 nm," Opt. Express **17**, 22773-22784 (2009).
24. D. L. Windt, J. F. Seely, B. Kjornrattanawanich, and Y. A. Uspenskii, "Terbium-based extreme ultraviolet multilayers," Opt. Lett. **30**, 3186-3188 (2005).
25. B. Kjornrattanawanich, D. L. Windt, and J. F. Seely, "Normal-incidence silicon–gadolinium multilayers for imaging at 63 nm wavelength," Opt. Lett. **33**, 965-967 (2008).
26. J. F. Seely, Y. A. Uspenskii, B. Kjornrattanawanich, and D. L. Windt, "Coated photodiode technique for the determination of the optical constants of reactive elements: La and Tb," SPIE Proc. **6317**, 63170T (2006).
27. M. G. Pelizzo, A. J. Corso, P. Zuppella, P. Nicolosi, S. Fineschi, J. Seely, B. Kjornrattanawanich, and D. L. Windt, "Long-term stability of Mg/SiC multilayers," Opt. Eng. **51**, 023801 (2012).
28. R. Soufli, M. Fernández-Perea, S. L. Baker, J. C. Robinson, J. Alameda, and C. C. Walton, "Spontaneously intermixed Al-Mg barriers enable corrosion-resistant Mg/SiC multilayer coatings," Appl. Phys. Lett. **101**, 043111 (2012).
29. M. Vidal-Dasilva, A. L. Aquila, E. M. Gullikson, F. Salmassi, and J. I. Larruquert, "Optical constants of magnetron-sputtered magnesium films in the 25–1300 eV energy range," J. Appl. Phys. **108**, 063517 (2010).
30. E. Shiles, T. Sasaki, M. Inokuti, and D. Y. Smith, "Self-consistency and sum-rule tests in the Kramers-Kronig analysis of optical data: Applications to aluminum," Phys. Rev. B **22**, 1612-1628 (1980), as compiled by E. D. Palik, *Handbook of optical constants of solids* (Academic Press, 1985).
31. R. Soufli and E. M. Gullikson, "Reflectance measurements on clean surfaces for the determination of optical constants of silicon in the extreme ultraviolet-soft-x-ray region," Appl. Opt. **36**, 5499-5507 (1997).

32. H. R. Philipp, "Influence of Oxide Layers on the Determination of the Optical Properties of Silicon," J. Appl. Phys. **43**, 2835-2839 (1972), as compiled by E. D. Palik, *Handbook of optical constants of solids* (Academic Press, 1985).
33. M. Fernández-Perea, J. I. Larruquert, J. A. Aznárez, J. A. Méndez, L. Poletto, A. M. Malvezzi, A. Giglia, and S. Nannarone, "Determination of optical constants of scandium films in the 20-1000 eV range," J. Opt. Soc. Am. A **23**, 2880-2887 (2006).
34. D. L. Windt, "IMD: Software for modeling the optical properties of multilayer films," Computers in Physics **12**, 360–370 (1998). Available at http://www.rxollc.com/idl/index.html.
35. J. B. Kortright and D. L. Windt, "Amorphous silicon carbide coatings for extreme ultraviolet optics," Appl. Opt. **27**, 2841-2846 (1988).
36. D. T. Attwood, *Soft X-Rays And Extreme Ultraviolet Radiation: Principles And Applications* (Cambridge University Press, 1999).
37. The observation that the thickness of the intermixed Al-Mg layer is approximately equal to the sum of the thicknesses of the constituent Al and Mg layers was made in Ref. [28] for Al and Mg thicknesses of 20 and 19 nm, respectively. This assumption may not hold for Al and Mg layers in different thickness ranges. At the time of writing of this manuscript, this is the best assumption that can be made based on experimental evidence.
38. R. Soufli, R. M. Hudyma, E. Spiller, E. M. Gullikson, M. A. Schmidt, J. C. Robinson, S. L. Baker, C. C. Walton, and J. S. Taylor, "Sub-diffraction-limited multilayer coatings for the 0.3 numerical aperture micro-exposure tool for extreme ultraviolet lithography," Appl. Opt. **46**, 3736-3746 (2007).
39. G. G. Stoney, "The tension of metallic films deposited by electrolysis," Proc. R. Soc. London, Ser. A **82**, 172-175 (1909).
40. J. H. Underwood and E. M. Gullikson, "High-resolution, high-flux, user friendly VLS beamline at the ALS for the 50-1300 eV energy region," J.Electr. Spectr. Rel. Phenom. **92**, 265-272 (1998).
41. E. M. Gullikson, S. Mrowka, and B. B. Kaufmann, "Recent developments in EUV reflectometry at the Advanced Light Source," SPIE Proc. **4343**, 363-373 (2001).
42. J. I. Larruquert, M. Vidal-Dasilva, S. García-Cortés, L. Rodríguez-de Marcos, M. Fernández-Perea, J. A. Aznárez, J. A. Méndez, "Multilayer coatings for the far and extreme ultraviolet", Proc. SPIE **8076**, 80760D (2011).

1. Introduction

In recent years, multilayer coatings with high near-normal-incidence reflectance in the extreme ultraviolet (EUV), defined here as the wavelength region from 10 to 100 nm, have enabled tremendous advances in the development of instrumentation for a wide range of applications and disciplines, from microchip production with EUV lithography to the observation of solar processes with space-borne telescopes. The 25-80 nm wavelength region is of particular relevance to many rapidly growing technological and scientific fields, such as solar physics [1,2] synchrotron and free electron laser facilities [3] and other EUV sources such as table-top capillary discharge lasers [4]. Some applications of EUV sources emitting in the 25-80 nm wavelength range include plasma physics [5], the characterization of materials and optical elements [6,7] materials damage [3], photochemistry of biological molecules [8], nanopatterning [9], and ultrafast single-shot microscopy[10].

As will be explained in more detail in Section 2, most material pairs used in multilayers for the EUV have a limited wavelength region of operation where narrowband peaks with high reflectance can be obtained, and outside of this region they become strongly absorbent. This explains why the use of "stacked" or large-period multilayers with multiple reflectance peaks has not been widely explored, with only a few exceptions [11,12]. In the case of mirrors for EUV solar imaging telescopes, a common solution that has been adopted in order to image several EUV emission lines using a single telescope consists in dividing each mirror in multiple sectors, with each sector tuned to one specific wavelength and coated separately using the appropriate material pair [13]. As a result, the instrument throughput corresponding to each wavelength is decreased accordingly. Moreover, this approach requires the use of a hardware mask placed on top of the mirror during multilayer deposition, which involves additional complexities and risks due to the proximity of the mask to the area being coated. "Shadowing" effects between the edges of the mask and the sector being coated diminish the multilayer performance and reduce the overall effective area of the mirror [14-16]. Multiple

telescopes often need to be employed in a given mission in order to achieve the number of EUV channels required to accomplish the science objectives [13]. This comes at the expense of increased payload mass, with mass being one of the most critical considerations towards the feasibility of a space mission. The development of multilayer coatings with high reflectance in multiple narrow wavelength bands could mitigate the aforementioned issues. Such multiple-wavelength coatings could be deposited on telescope mirrors and combined with the appropriate filters for wavelength selection, or be used as part of a spectrometer instrument.

Mg/SiC is a remarkable material pair because (i) Mg absorption remains relatively low across a wide EUV wavelength range, beginning at 25 nm (the Mg 2p edge) and extending up to about 115 nm, (ii) there is good optical contrast between the Mg and SiC materials, and (iii) the Mg-SiC interfaces are sharp and stable. This allows for efficient and simultaneous reflection of radiation in multiple narrow bands centered at wavelengths in the spectral region from 25 to 80 nm. In addition to this, Mg/SiC possesses several other favorable properties: near-zero film stress, good spectral selectivity and thermal stability up to about 350° C [17,18]. This unique combination of properties is highly desirable for mirror multilayer coatings in solar physics instrumentation and is unmatched by any of the other multilayer material pairs operating in the > 25 nm wavelength region such as Mo/Si [19], SiC/Si [19], Sc/Si [20], B4C/Si [19], Al/SiC [21], other Mg-based multilayers such as Mg/Co [22], and rare-earth based multilayers [23-26]. Despite the superior optical performance of Mg/SiC multilayers in the EUV region when compared to other material pairs, their use as coatings in applications that require long-term stability, such as for example the EUV imaging telescopes aboard NASA's Solar Dynamics Observatory mission [14], has been hindered by Mg corrosion [15,27]. Corrosion occurs in Mg/SiC multilayers after long-term exposure to the atmosphere, and appears as corroded areas on the top surface which are visible to the eye and have completely degraded (near-zero) EUV reflectance. The origins and propagation of corrosion in Mg/SiC multilayer coatings have been recently elucidated [28]. It was determined that, for coatings deposited on sufficiently clean substrates, corrosion starts from the top of the multilayer structure and is caused by Mg interacting with environmental agents, which reach the Mg layers buried under the SiC capping layer through pinholes and other defects typical of magnetron-sputtered thin films, and also through defects generated by sample manipulation, such as scratches. The atmospheric corrosion of Mg/SiC multilayers was dramatically reduced by depositing an Al thin film of optimized thickness on top of the last (topmost) Mg film in the multilayer, underneath the SiC capping layer [28]. The Al and Mg layers spontaneously intermix to form a partially amorphous Al-Mg layer which provides efficient corrosion protection while, due to the Al transparency below 83 nm, maintaining the favorable optical properties of the original, unprotected Mg/SiC multilayer. The efficacy of this corrosion protection concept was verified experimentally on Mg/SiC films aged for 3 years. It has been postulated [28] that the corrosion protection capabilities of the Al-Mg layer are greatly enhanced by its spontaneous amorphization, which results in reduced grain boundaries, vacancies and defects and thus reduced permeability to humidity, oxygen (O^{2-}) and other reactive ions.

In this work we make use of both the wide-band transparency of Mg and Al in the EUV and the corrosion resistance afforded by Al-Mg layers to produce efficient, triple-wavelength, normal-incidence Mg/SiC multilayer coatings with corrosion resistance for the spectral region from 25 to 80 nm. We propose two different candidate concepts for corrosion resistance based on the deposition of an Al-Mg layer (i) on top of the multilayer and (ii) in each period in the multilayer. Furthermore, a design concept where an Al layer is deposited on top of a SiC layer (to deliberately avoid spontaneous intermixing with Mg) has been produced. The reflectance of these coatings was measured and modeled in an extended wavelength range (11.2 – 186.1 nm), to assess their in-band and off-band performance. This manuscript is focused on the experimental demonstration of the reflective properties of triple-wavelength Mg/SiC

multilayers, equipped with candidate concepts for corrosion-resistance. The relative efficacy of the various corrosion-resistance concepts is currently being monitored and will be presented in detail in a future publication, to allow sufficient time for the aging of these samples. For comparison purposes, we also present the design and experimental reflectance of a standard (unprotected), triple-wavelength Mg/SiC multilayer. The same concepts used here to demonstrate triple-wavelength coatings can also be adapted for single- and double-wavelength applications.

2. Multilayer design

Photon energies in the EUV region approach the binding energies of atomic core electrons, making all materials strongly absorbent. Multilayer designers have traditionally made use of the relatively lower absorption of materials at wavelengths just slightly longer than their absorption edges. However, most materials soon become strongly absorbent again at wavelengths further away from the absorption edge, limiting the spectral range of application of each material pair. That is the reason why a combination of different material pairs has to be used in order to cover the entire EUV range. In Fig.1 the extinction coefficient of three materials commonly used as spacers for multilayers in the EUV is compared with that of Mg.

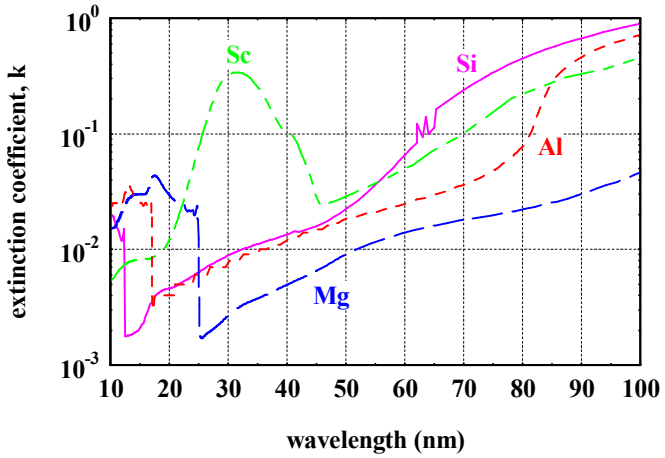

Fig. 1. (Color online) Extinction coefficient of several materials widely used as spacers for multilayers in the EUV. Mg shows the lowest extinction coefficient values in the EUV above the Mg 2p edge at 25 nm. Notice that Al also exhibits relatively low absorption between the Al 2p edge at 17 nm and the Al plasma wavelength at 83 nm.

Extinction coefficient values were obtained from Ref. [29] for Mg, Ref. [30] for Al, Refs. [31] and [32] for Si, and Ref. [33] for Sc. Among this group of materials, Mg is by far the less absorptive material for all EUV wavelengths longer than 25 nm. Depending on the wavelength, the extinction coefficient of Mg is between 2 and 15 times smaller than that of Al, between 2 and 22 times smaller than that of Si and between 3 and 100 times smaller than that of Sc. The transparency of Mg over a wide wavelength range, as shown in Fig. 1, makes it suitable for use in multiple-wavelength multilayer designs.

Fig. 2 shows two-dimensional contour plots of calculated near-normal-incidence reflectance as a function of both wavelength and multilayer period, for (a) standard Mg/SiC multilayers, (b) Mg/SiC multilayers where the topmost Mg layer has been replaced by an Al-Mg layer, and (c) (Al-Mg)/SiC multilayers. All multilayers have N=40 layer pairs. The ratio of the thickness of the spacer (either Mg or Al-Mg) to the multilayer period (Γ), is shown in Fig. 2 for each case. In Figs. 2(a) and 2(c) Γ was selected to maximize the reflectance of the first reflectance order, while keeping the second and third ones as high as possible. In Fig. 2(b), Γ was increased further in order to enhance the reflectivity of the higher orders, which

would otherwise be very small. The plots in Fig. 2 should be considered as examples, and the Γ value could be selected according to application-specific considerations. All multilayers include a SiC capping layer 9 nm thick. The calculations in Fig. 2 were performed assuming layer interfaces with roughness values obtained from fits to measured reflectance values (see Section 4 and Table 1). The Al-Mg layer thickness used in the calculations of Fig. 2(b) was assumed to be equal to the thickness of the Mg layers. The optimum Al-Mg thickness would have to be calculated for each multilayer period value, and will depend on the specifics of each application. Reflectance values were calculated using the IMD software [34], with experimental optical constants values obtained from Ref. [29] for Mg, Ref. [35] for SiC and Ref. [30] for Al. We assumed uniform Al-Mg layers formed after the subsequent deposition of two Al and Mg layers of equal thickness, which is equivalent to a 60.8 wt. % content of Al. Since no optical constants are available for the Al-Mg layers, we calculated the optical constants of the composite material from those of pure Al and Mg. The Al weight percentage was selected rather arbitrarily, and in practice could be different. As a general trend, the performance of all coatings improves with decreasing percentages of Al in the Al-Mg layer, but a minimum Al weight percentage will be required to achieve efficient corrosion protection, depending on the environmental conditions of the application.

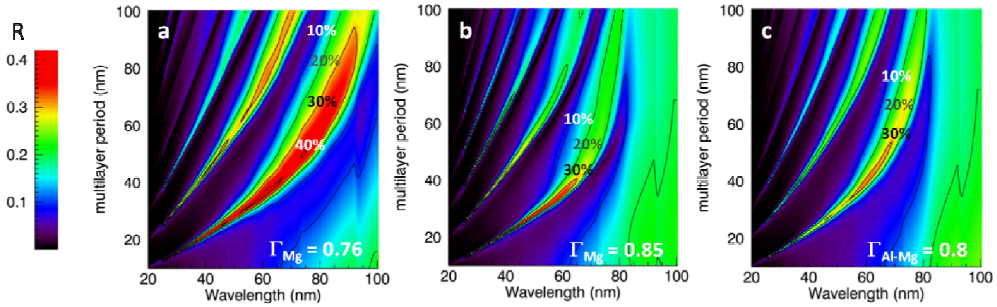

Fig. 2. (Color online) Two-dimensional, calculated [34] contour plots of near-normal-incidence (θ = 85°) reflectance (R) as a function of both wavelength and multilayer period, for (a) standard Mg/SiC multilayers ([SiC/Mg]x40/SiC), (b) Mg/SiC multilayers where the topmost Mg layer has been replaced by an Al-Mg layer of optimized thickness ([SiC/Mg]x39/SiC/Al-Mg/SiC), and (c) (Al-Mg)/SiC multilayers ([SiC/Al-Mg]x40/SiC).

In order to calculate the optical constants of the Al-Mg layers, atomic scattering factors were calculated from the optical constants of the pure materials, as shown in Eqs. (1) and (2):

$$f_1 \cong \frac{2\pi}{n_a r_e \lambda^2}(1-n), \tag{1}$$

$$f_2 \cong \frac{2\pi}{n_a r_e \lambda^2} k. \tag{2}$$

Where f_1 and f_2 are the real and imaginary parts of the atomic scattering factor, n_a is the atomic density, r_e is the electron radius, λ is the wavelength and n and k are the real and imaginary parts of the index of refraction. These equations were used separately for both Al and Mg. For the atomic density calculation, Al and Mg mass densities were assumed to be 2.70 gcm^{-3} and 1.74 gcm^{-3}, respectively. The optical constants of the Al-Mg layer were obtained from the expressions:

$$n(Al-Mg) \cong 1 - \frac{r_e \lambda^2}{2\pi}[\tilde{n}_a(Al) f_1(Al) + \tilde{n}_a(Mg) f_1(Mg)], \tag{3}$$

$$k(Al-Mg) \cong 1 - \frac{r_e \lambda^2}{2\pi}[\tilde{n}_a(Al) f_2(Al) + \tilde{n}_a(Mg) f_2(Mg)]. \tag{4}$$

Where $\tilde{n}_a$ corresponds to the atomic density of each species in the Al-Mg layer. Eqs. (1) to (4) are valid under two assumptions, (i) that n ≈1 and k << 1, and (ii) that the independent atom approximation for the atomic scattering factors is valid. Both conditions hold strictly at wavelengths shorter than ~30 nm and away from absorption edges [36], but we used them as the best approximation currently available at wavelengths up to 120 nm. We calculated the Al and Mg atomic densities in the Al-Mg layer based on earlier observations of cross-sectional TEM images, which showed no significant expansion or contraction of the total thickness after spontaneous intermixing of the Al and Mg layers [28,37].

We have deposited and characterized one sample corresponding to each of the design concepts proposed in Fig. 2, plus an additional concept that uses Al instead of Al-Mg as a candidate corrosion protective layer. Details on sample preparation and characterization methods are given in the next section.

3. Experimental techniques

All multilayer films were deposited in a planar DC-magnetron sputtering deposition system [38] located at Lawrence Livermore National Laboratory (LLNL), on 100 mm-diameter, 525 μm-thickness ultra-smooth (<0.1 nm rms high-spatial frequency roughness) Si substrates with (100) orientation. During deposition, each Si wafer substrate was mounted on a platter which passes underneath the sputtering material sources (targets) in a rotational motion at velocities on the order of 1 rpm. An algorithm based on modulation of the rotational velocity of the platter is used to control the coating thickness and to achieve the required coating thickness uniformity in the radial direction. Each substrate was also spinning around its center at 400 rpm, to achieve thickness uniformity in the azimuth direction. The base vacuum pressure in the deposition chamber was in the range 2×10^{-8} - 3×10^{-8} Torr and argon (Ar) was used as process gas at 10^{-3} Torr. The dimensions of each sputtering target were 127 × 559 mm^2 and the quoted target purity was 99.97 wt. % for Mg, 99.9999 wt. % for SiC and 99.9995 wt. % for Al. During deposition, the sputtering targets operated at constant power: 1200 W (Mg), 1000 W (SiC) and 2000 W (Al).

The thin film stress properties of Mg/SiC multilayers were measured at LLNL using a Tencor FLX-2320TM stress-measuring apparatus that uses laser beams at 650 nm and 750 nm wavelengths to measure the radius of curvature of the substrate before and after coating. These measurements are employed in a modified Stoney [39] equation to calculate the thin film stress.

EUV reflectance measurements in the wavelength range 11.2-49.5 nm were performed at beamline 6.3.2. of the Advance Light Source (ALS) synchrotron at Lawrence Berkeley National Laboratory (LBNL). The general characteristics of the beamline have been described in detail earlier [40,41]. Two gratings (80 and 200 lines/mm) were used in the monochromator to access the wavelength range 11-50 nm. The monochromator exit slit was set to a width of 40 μm. Wavelength calibration was based on the 2p absorption edges of Al and Si transmission filters with a relative accuracy of 0.011% rms, and could be determined with 0.007% repeatability. During the measurements, 2nd harmonic and stray light suppression was achieved with a series of transmission filters (Mg, Al, Si, Be). For higher-order harmonic suppression, an "order suppressor" consisting of three carbon-coated mirrors at a variable grazing incidence angle (depending on wavelength range) and based on the principle of total external reflection was used in addition to the filters. The ALS storage ring current was used to normalize the signal against the storage ring current decay. The signal was collected on a GaAsP photodiode detector, with 1º angular acceptance. Reflectance was measured with ±1% relative accuracy, dominated by the GaAsP photodiode uniformity in each wavelength range. The vacuum pressure in the measurement chamber was in the range 2×10^{-6} - 10^{-7} Torr.

Reflectance measurements at 48.9-186.1 nm wavelengths were performed at Grupo de Óptica de Láminas Delgadas (GOLD). The monochromator consists of a lamp and a grazing

incidence toroidal-grating monochromator, covering the 12.5-200 nm range. It has two Pt-coated diffraction gratings, 250 and 950 lines/mm. The entrance-exit arms are 146º apart. A windowless discharge lamp is used to generate spectral lines that cover the range longer than ~40 nm. The lamp is fed with a variety of pure gases such as Ar, He or CO_2, or gas mixtures consisting of noble gases, along with N_2 or H_2. In most cases radiation corresponds to a single spectral line (except for a low background) since adjacent spectral lines are rejected by the monochromator. The beam divergence was ~5 mrad and angle accuracy is estimated as ±0.1º. Samples up to 50.8×50.8 mm^2 can be loaded in the sample holder, from which a rectangle of 50.8×25 mm^2 can be scanned. The detector is a channel electron multiplier with a CsI-coated photocathode. Reflectance was obtained by the alternate measurement of the incident intensity and the intensity reflected by the sample, with accuracy estimated as ±1%. A more detailed description of this system can be found elsewhere [42].

4. Results and discussion

Four different multilayers were deposited and measured: three according to the design concepts shown in Fig. 2 (a), (b) and (c), plus an additional sample where we used Al instead of Al-Mg, to later explore its potential as protective layer against corrosion. All the corrosion-resistant designs included a 20 nm-thick Al layer at the bottom of the multilayer structure, for additional corrosion protection from contamination that could potentially exist on the substrate. The bottom Al layer could be deposited either as a separate layer below the first SiC layer, or below the first (bottom) Mg layer to produce an intermixed Al-Mg layer. The multilayer parameters were selected so that the first order reflectance peak would be located at wavelengths between 55 to 80 nm. All EUV reflectance measurements were performed within a period of 1 to 3 months after deposition of the samples.

Fig. 3 shows the near-normal-incidence (θ = 85°) reflectance measurements on the standard unprotected Mg/SiC multilayer, along with calculated values corresponding to a model with parameters as shown in Table 1.

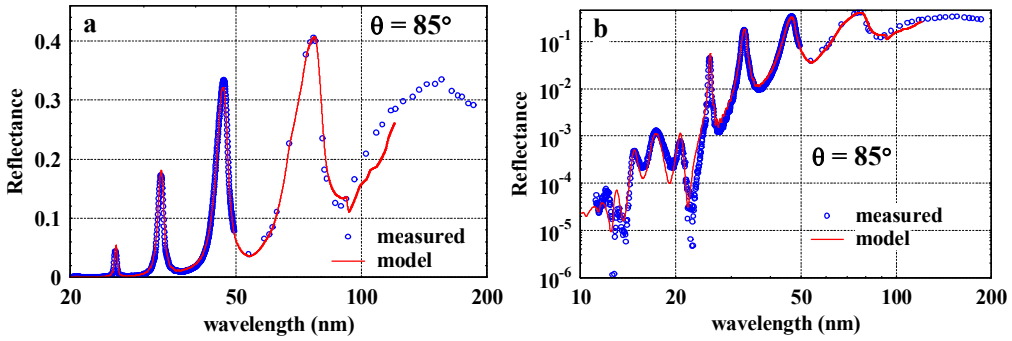

Fig. 3. (Color online) Experimental reflectance of standard (unprotected) Mg/SiC multilayer showing a) the first four reflectance orders in log-linear scale and b) data spanning 5 orders of magnitude in log-log scale. Calculated values [34], corresponding to a model with parameters as shown in Table 1, are also included as a solid line. A record narrowband peak reflectance value of 40.6% was obtained at 76.9 nm.

This sample was deposited for comparison with the candidate corrosion-resistant designs. The measurements performed at GOLD included one wavelength at 48.9 nm, overlapping with the ALS wavelength range. Considering the reflectance uncertainties, both measured reflectance values are identical, confirming the consistency between the measurements performed at the two facilities. The first three reflectance orders were measured at peak wavelengths of 76.9, 46.8 and 33.1 nm, with reflectance values of 40.6% (15), 33.4% (3.6) and 17.2% (1.2), respectively, where the FWHM in nm is indicated in parentheses. The wide spectral range covered by the measurements allows for a good understanding of the out-of-band contributions at long wavelengths. In all the following calculations, the same Mg and

SiC optical constants were used as in the calculations shown in Fig. 2, which in the case of SiC cover wavelengths only up to 120 nm. However, only optical constant values up to about 85 nm are in good agreement with our measurements, as is shown by the large difference between the measured and modeled reflectance values for wavelengths between 85 and 120 nm. This is not surprising since it is known that thin film optical properties are strongly dependent on deposition methods and storage environment, and that the effect of oxides that may be present on the top surface of the thin films is especially pronounced at long wavelengths. Fig. 3(b), in logarithmic scale, shows detailed reflectance fine structure spanning 5 orders of magnitude, from 0.406 to 1.1×10^{-6}. Even though Mg/SiC multilayers have been extensively studied in the past for EUV applications, to our knowledge this is the first time they are reported to work efficiently at wavelengths as long as 76.9 nm. In addition, the measured reflectivity value of 40.6% is the highest reported so far for a narrowband multilayer peak at this wavelength.

Table 1. Coating parameters corresponding to the models shown as red solid lines in Figs. 3 and 4. The multilayer structure is specified from the bottom to the top of the sample. All thickness (period, *d*) and roughness (σ) values are given in nm and nm rms, respectively. The thickness of the base Al layer (Al′) is 20 nm. Γ is the ratio of Mg (or Al-Mg) thickness to the total period thickness. σ′ and σ″ represent the roughness in nm of the Mg (or Al-Mg) on SiC and SiC on Mg (or Al-Mg) multilayer interfaces, respectively. The multilayers were designed to have the 1st order reflectance peak at 75, 75, 65 and 55 nm wavelengths.

Multilayer structure	Period	Γ	N	σ′	σ″	*d*(SiC′)	*d*(Al-Mg′) or *d*(Al″)	*d*(SiC″)
[SiC/Mg]xN/SiC″	52.4	0.77	10	0.5	2.0	0	0	10.8
Al′/[SiC/Mg]xN/ SiC′/Al-Mg′/SiC″	52.2	0.78	9	0.3	1.8	11.8	45.0	9.5
Al′/[SiC/Al-Mg]xN/ SiC″	45.0	0.79	10	0.8	1.8	0	0	8.8
Al′/[SiC/Mg]xN/ SiC′/Al″/SiC″	31.5	0.75	35	0.5	0.8	6.2	30.9	9.2

Fig. 4 shows the near-normal-incidence (θ = 85°) reflectance measurements on candidate corrosion-resistant designs, along with calculated values corresponding to the model parameters in Table 1. The sample in Fig. 4(a) included an Al-Mg layer (15.3 wt. % of Al) in place of the topmost Mg layer in the multilayer stack. This layer was deposited as two consecutive layers with nominal thicknesses of 38.6 nm of Mg (first layer) and 4.5 nm of Al (second layer). The Al weight percentage was chosen to be relatively small in this case, in order to maximize the reflectance at longer wavelengths where Al becomes more absorbent, and also to test the corrosion resistance provided by Al-Mg layers of varied composition. Optical constants of the Al-Mg layer, needed for modeling purposes, were calculated from Al and Mg atomic scattering factors following the method outlined in Section 2. A SiC capping layer was deposited on top of the Al-Mg layer for additional protection from corrosion and oxidation. The first three reflectance orders were measured at peak wavelengths of 76.0, 46.9 and 33.1 nm, with reflectance values of 38.0% (14.1), 30.0% (3.6) and 15.4% (1.2), respectively, where the FWHM in nm is indicated in parentheses. With reflectance values of only a couple of percentage points lower than that of the standard Mg/SiC sample in Fig. 3, this multilayer has the potential to offer improved corrosion resistance with almost identical peak reflectance and FWHM. The agreement between the measurement and the model at wavelengths between 30 and 85 nm is remarkable, considering the approximations used in the Al-Mg optical constants calculations. Above 85 nm the model doesn't predict the measurements correctly, presumably for the same reason as in Fig.3, i.e. possible inaccuracies of the optical constants and/or of the model parameters for the top layer of the multilayer. It may be worthwhile mentioning that the three peak wavelengths in this multilayer sample nearly coincide with EUV solar emission lines: O IV/Ne VIII (78 nm, 1st order), Ne VII (46.5 nm, 2nd order) and Fe XVI (33.5 nm, 3rd order). The 2nd and 3rd orders provide superior

spectral selectivity combined with high reflectivity. The above illustrate the suitability of these multilayers as triple-wavelength mirror coatings for solar physics.

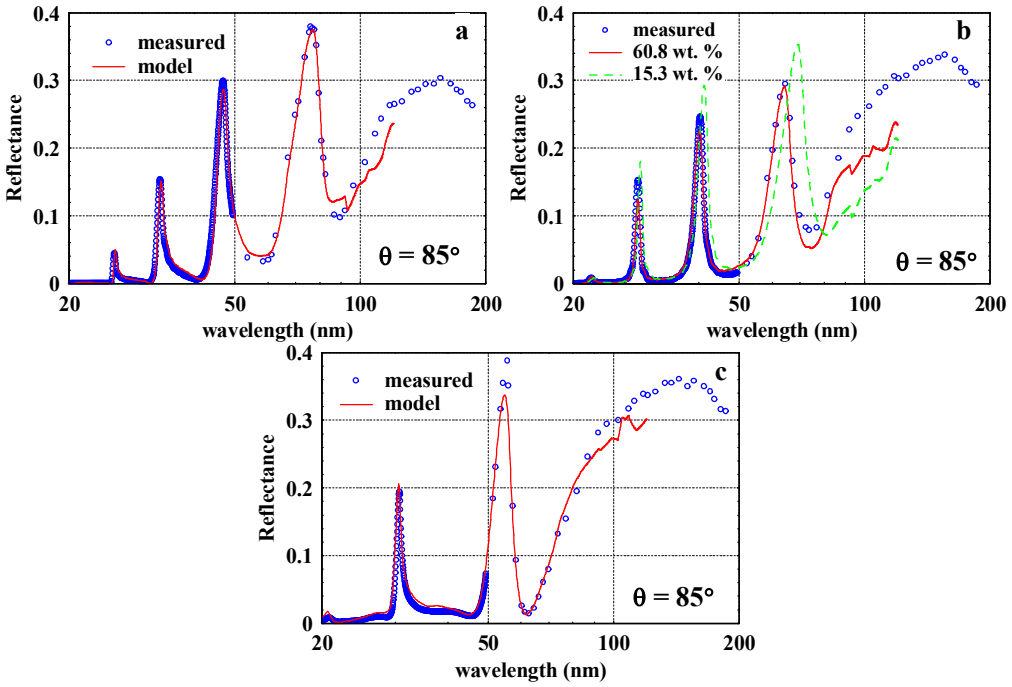

Fig. 4: (Color online) Experimental reflectance of candidate corrosion-resistant, multiple-wavelength Mg/SiC multilayer concepts where a) the topmost Mg layer has been replaced by an Al-Mg layer with 15.3 wt. % of Al, b) each Mg layer has been replaced by an Al-Mg layer with 60.8 wt. % of Al, and c) the topmost Mg layer has been replaced by an Al layer. All plots include calculated [34] values corresponding to models with parameters as shown in Table 1. In b) the performance of a multilayer with the same thickness and roughness parameters but with a 15.3 wt. % of Al in the Al-Mg layers was also calculated and is shown for the purpose of illustrating the potential of this concept towards high peak reflectance.

The sample in Fig. 4(b) included an Al-Mg layer in each period, obtained by depositing two consecutive Mg and Al layers of equal thickness, which results in 60.8 wt. % of Al. The Al weight percentage was chosen to be nearly the same as in Ref. [28], which has been proven to provide efficient corrosion resistance for at least three years. The Al-Mg optical constants were calculated as explained earlier in Section 2. A smaller multilayer period thickness was selected in order to shift the peak wavelengths towards shorter values. The first three reflectance orders were measured at peak wavelengths of 64.5, 40.4 and 28.6 nm, with reflectance values of 29.5% (9.6), 24.6% (2.2) and 15.3% (0.9), respectively (FWHM in nm is indicated in parentheses). The model values, labeled as "60.8 wt. %" in Fig. 4(b), agree with the measured data only up to ~66 nm. This may be an indication that the Al-Mg layer model, which assumes uniform composition, is not accurate. To illustrate the potential of this design in achieving the highest possible peak reflectance values we also included a calculation of the expected reflectance of a multilayer with the same thickness and roughness parameters but Al-Mg layers with 15.3 wt. % of Al (as the one used in the multilayer of Fig. 4(a)). The result is labeled in Fig. 4(b) as "15.3 wt. %". The first three reflectance orders are predicted at peak wavelengths of 69.1, 41.2 and 29.0 nm, with reflectance values of 35.3%, 29.3% and 18.0%, respectively. Therefore, when reducing the Al content from 60.8 to 15.3 wt. % of Al, the peak reflectance is expected to increase 6, 5 and 3 absolute percentage points at the first, second and third reflectance peaks, respectively. These values are very similar to those obtained in the case of the sample in Fig. 4(a), but since the Al-Mg layer is present in each period, the corrosion resistance of the sample in Fig. 4(b) could be even better. The sample in Fig. 4(c)

included an Al layer deposited instead of the topmost Mg layer in the multilayer. Due to the different optical constants of Mg and Al, the thickness of both the Al and the SiC layer underneath the Al layer were modified in order to optimize the reflectance response. Optical constants of Al were obtained as before from Ref. [30]. An even smaller multilayer period thickness was selected in order to shift the peak wavelengths towards even shorter values. As a consequence this multilayer only presents two reflectance peaks at wavelengths of 55.7 and 30.7 nm, with reflectance values of 38.8% (5.6) and 19.4% (1.1), respectively (FWHM in nm is indicated in parentheses). In this case it was not possible to model the measured reflectance adequately at the first order reflectance peak between 52 and 57 nm. This could be caused by inaccuracies in the model parameters or in the optical constants, possibly of Al. As before, at longer wavelengths the model disagrees with the measured values above 85 nm. Stress measurements performed on the samples in Figs. 3, 4(a) and 4(b) demonstrated moderate compressive stress values of -158 , -134 and -169 MPa, respectively.

5. Conclusions

Based on the transparency of Al and Mg at EUV wavelengths longer than 25 nm and the enhanced corrosion resistance provided by Al-Mg layers, we have developed two candidate concepts for corrosion-resistant, triple-wavelength Mg/SiC multilayer designs for operation in the spectral range from 25 to 85 nm. A third candidate design including an Al layer at the top of the multilayer (underneath the SiC capping layer) instead of the Al-Mg layer was also deposited. In addition, a standard Mg/SiC multilayer was deposited and measured for comparison purposes. The reflectance of all samples was measured at near-normal incidence between 11.2 and 186 nm and high peak reflectance across the 1^{st}, 2^{nd} and 3^{rd} interference orders of all four multilayer samples was demonstrated, including a record narrowband reflectance value of 40.6% at 76.9 nm in the case of the standard Mg/SiC sample. Theoretical models were developed for all samples, which predicted the measured performance accurately over an extended wavelength range, making possible the design of multilayers with other Al-Mg layer compositions and Γ values. Aperiodic or "stacked" Mg/SiC multilayer designs using the concepts discussed in this manuscript are also possible, to customize the reflectance peaks of these multilayers to exactly coincide with specific EUV plasma emission lines.

The corrosion resistance and lifetime properties of all samples are currently being monitored and will be discussed in a future publication. Of particular interest is the question of the minimum wt. % of Al required for long-term Mg/SiC corrosion resistance, which may depend on the deposition and storage conditions (e.g: humidity) of the multilayer samples. The proposed Mg/SiC corrosion-resistant coatings are highly relevant to EUV applications where long lifetime stability is needed, such as space-borne solar physics missions. Such missions may additionally benefit from the decreased payload mass and ease in multilayer fabrication resulting from the triple-wavelength multilayer reflective performance.

Acknowledgments

This work was performed under the auspices of the U.S. Department of Energy by Lawrence Livermore National Laboratory under Contract No. DE-AC52-07NA27344 and by the University of California Lawrence Berkeley National Laboratory under Contract No. DE-AC03-76F00098. The Advanced Light Source is supported by the Director, Office of Science, Office of Basic Energy Sciences, of the U.S. Department of Energy under Contract No. DE-AC02-05CH11231. Funding was provided in part by LLNL's Laboratory Directed Research and Development Program. GOLD acknowledges financial support from the National Program for Space Research, Subdirección General de Proyectos de Investigación, Ministerio de Ciencia y Tecnología, project number AYA2010-22032.